Electrochemical Detection of Faraday Waves on the Surface of a Gas Bubble

Peter R. Birkin,*,† Yvonne E. Watson,† Timothy G. Leighton,‡ and Karen L. Smith†

Department of Chemistry, and Institute of Sound and Vibrational Research, University of Southampton, Highfield, Southampton, SO17 1BJ, United Kingdom

Received July 16, 2001. In Final Form: November 13, 2001

The oscillation of a gas bubble driven by an acoustic field has been investigated using an electrochemical sensing technique. A low-resolution scanning electrochemical microscopy technique, employing an L-shaped microelectrode, has been employed to address the equator of a tethered bubble. Real-time mass transfer enhancements as the result of bubble wall motion have been detected using the electrochemical reduction of $Fe(CN)_6^{3-}$. A comparison of the pressure threshold measurements of the onset of surface oscillations with a theoretical model is presented. Photographic evidence of the presence and shape distortions of the bubble surface is also demonstrated.

Introduction

The investigation of the interface between different phases of matter is extremely important in understanding many physical, chemical, and biological processes.[1−3] Hence, many investigations have targeted phase interfaces using electrochemical techniques as this provides useful data on the physical and chemical nature of the interface.[4−6] Among the many studies, the employment of scanning electrochemical microscopy (SECM[7]) has yielded some of the most interesting insights into the nature of phase interfaces between liquids and between liquids and gases.[8−13] In most instances, the interface under investigation has been macroscopic in nature (e.g., a planar interface between two liquids) while inclusions within another phase (e.g., gas bubbles) have not been investigated to the same extent.

The study of bubbles within liquids is extremely important in understanding many processes which occur naturally. As an example, the exchange of gases between the atmosphere and the ocean is thought to involve bubble entrapment within the surface.[14] Clearly, the investigation of the physical and chemical processes at the liquid/gas interface of bubbles is extremely important.

One of the key physical effects of bubbles is their interaction with sound. Irradiation of a bubble with sound of the appropriate frequency leads to a number of interesting physical processes including sound absorption, scattering, and bubble motion. One such process can be described as "surface waves". Faraday, in 1831, first noted that it was possible to initiate surface waves with a frequency of half the original driving oscillation.[15] These "Faraday waves" are known to occur when the amplitude of oscillation of the liquid/gas interface exceeds a threshold value. Faraday waves can be excited on the wall of a gas bubble, since an applied sound field can drive the bubble into resonant pulsation. The amplitude of wall pulsation can be increased either by fixing the frequency of the applied field and increasing its acoustic pressure amplitude or by fixing the amplitude of the sound field and tuning the frequency to be closer to the bubble resonance.[16−18] A useful application from this is the ability to find a bubble resonance, and hence its size, by sweeping the frequency of the applied field until the bubble wall appears to "shimmer", corresponding to the visual detection of Faraday waves.

The ability to size bubbles has a wide range of applications, from the characterization of medical echocontrast agents used in forming ultrasonic images, to the study of the mass flux between atmosphere and ocean, to applications in the manufacture of foodstuffs and pharmaceuticals.[14] The resonant bubble pulsation is commonly used, on the principle that the bubble scatters maximally when the applied field is tuned to the bubble resonance. The acoustic emissions from Faraday waves are very weak, since unlike the pulsation they do not give rise to a

* Corresponding author. E-mail: prb2@soton.ac.uk.
† Department of Chemistry.
‡ Institute of Sound and Vibrational Research.

(1) Adamson, A. W. *Physical Chemistry of Surfaces*; Wiley: New York, 1997.
(2) Somorjai, G. A. *Surface Chemistry and Catalysis*; Wiley: New York, 1994.
(3) Tsionsky, M.; Cardon, Z. G.; Bard, A. J.; Jackson, R. B. *Plant Physiol.* **1997**, *113*, 895.
(4) Bard, A. J.; Faulkner, L. R. *Electrochemical Methods*; Wiley: New York, 1980.
(5) Christensen, P. A.; Hamnett, A. *Techniques and Mechanisms in Electrochemistry*; Blackie: Glasgow, 1994.
(6) Bard, A. J.; Fan, F. R. F.; Kwak, J.; Lev, O. *Anal. Chem.* **1989**, *61*, 132.
(7) Kwak, J.; Bard, A. J. *Anal. Chem.* **1989**, *61*, 1221.
(8) Tsionsky, M.; Bard, A. J.; Mirkin, M. V. *J. Am. Chem. Soc.* **1997**, *119*, 10785.
(9) Delville, M. H.; Tsionsky, M.; Bard, A. J. *Langmuir* **1998**, *14*, 2774.
(10) Shao, Y.; Mirkin, M. V.; Rusling, J. F. *J. Phys. Chem. B* **1997**, *101*, 3202.
(11) Slevin, C. J.; Macpherson, J. V.; Unwin, P. R. *J. Phys. Chem. B* **1997**, *101*, 10851.
(12) Slevin, C. J.; Ryley, S.; Walton, D. J.; Unwin, P. R. *Langmuir* **1998**, *14*, 5331.
(13) Unwin, P. R. *J. Chem. Soc., Faraday Trans.* **1998**, *94*, 3183.
(14) Leighton, T. G. *The Acoustic Bubble*; Academic Press: London, 1994.
(15) Faraday, M. On the forms and states assumed by fluids in contact with vibrating elastic surfaces. *Philos. Trans. R. Soc.* **1831**, *121*, 319−340.
(16) Franscescutto, A.; Nabergoj, R. *Acustica* **1978**, *41*, 215.
(17) Phelps, A. D.; Leighton, T. G. *J. Acoust. Soc. Am.* **1996**, *99*, 1985.
(18) Phelps, A. D.; Leighton, T. G. *Acta Acust.* **1997**, *83*, 59.

10.1021/la0111001 CCC: $22.00
Published on Web 02/16/2002

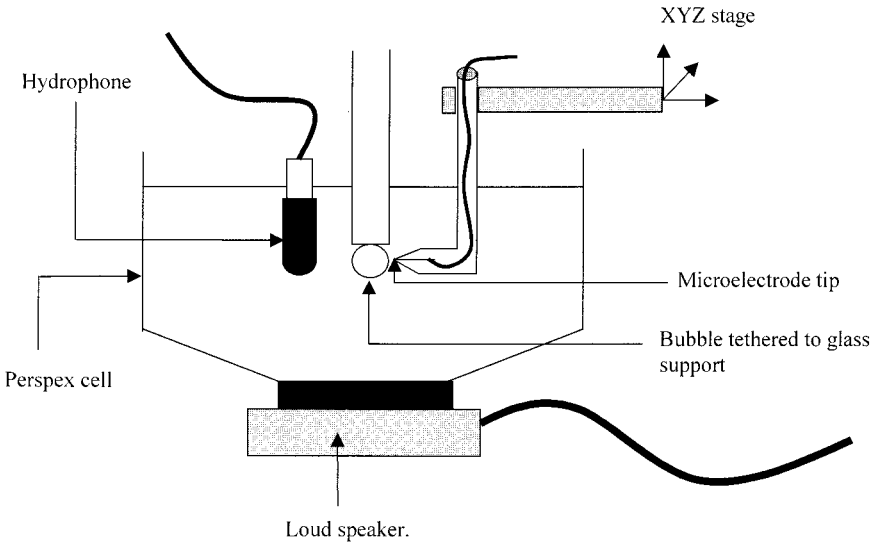

Figure 1. Schematic representation of the acoustoelectrochemical cell employed to study the surface waves on the bubble wall. The cell was not thermostated. The dimensions of the cell were 8.6 cm × 8.6 cm × 5 cm.

monopole acoustic emission. The only acoustic technique which has been successful in detecting these waves is a complicated procedure which involves two sound fields directed at the bubble; specifically, they can be detected by driving the bubble at resonance using a "pump" acoustic field, of frequency f_p (typically of kHz order), and scattering from that bubble an "imaging" sound field of frequency f_i ($\sim$ 1 MHz). The motion of the bubble wall modulates the scattered imaging signal at the frequency of the relevant wall motion (f_p for the pulsation; $f_p/2$ for the Faraday waves).[17,18] If the bubble is only pulsating, the high frequencies therefore contain f_i and $f_i \pm f_p$. If the pulsation amplitude has been sufficient to excite Faraday waves, then the high-frequency acoustic scatter contains, *in addition*, components at $f_i \pm f_p/2$. Though not robust in dense populations, the detection of $f_i \pm f_p/2$ provides the most precise way of sizing bubbles yet discovered.

Faraday waves on bubble walls therefore present a fascinating contradiction. They provide both the easiest (visual detection of shimmer) and probably most difficult ($f_i \pm f_p/2$) ways of sizing bubbles, and each has a role. The lack of a direct acoustic emission at $f_p/2$ adds to the intriguing nature of this phenomenon.

This paper presents, for the first time, a new way of detecting the onset of Faraday waves on bubble walls, using the effect of the wall motion on the electrochemistry at a nearby microelectrode. The electrochemical investigation of planar gas/liquid interfaces has been reported in the literature. Unwin et al., in an eloquent study, investigated the transfer of oxygen gas across a planar air/water interface.[12] In this case, the interface was initially "clean" and then was controllably covered with a layer of a surfactant. The kinetics of oxygen transfer across the planar interface was then investigated as a function of surface coverage. However, the investigation of the kinetics of gas transfer across an air/water interface of a bubble is beyond the scope of this paper and will be dealt with elsewhere.

The work presented in this manuscript as well as extending our knowledge on the fundamentals of bubble oscillations can be deployed to develop novel acoustoelectrochemical sensors. This combination of acoustics with electrochemical sensors can be potentially exploited to assess bubble populations within the ocean.[19,20]

In the study reported here, the motion of the bubble wall is investigated using a platinum 25 μm diameter microelectrode in a solution containing $Fe(CN)_6^{3-}$. The microelectrode is positioned close to (5−10 μm) the interface using a micrometer and stage. The motion of the bubble wall is then detected as an enhancement in mass transfer to the microelectrode.

Experimental Section

All electrochemical measurements are made using a two-electrode system comprising of 25 μm platinum working disk microelectrode sealed in glass and a silver counter/reference electrode. To address the gas liquid interface between the bubble wall and the solution, an L-shaped microelectrode was required. This enabled the equator of the bubble to be probed electrochemically. To fabricate this microelectrode, two slightly different experimental procedures were employed. In the first, an L-shaped glass tube was pulled into a capillary at one end and a microelectrode was fabricated as described previously.[21] The tip of the microelectrode could then be polished and shaped to a point ($R/G \sim 5$) as in conventional SECM practice.[6,7] In the second technique, a straight microelectrode was fabricated, polished, and shaped and then attached with epoxy resin at 90° to a glass support rod. These two fabrication techniques were successful in producing robust microelectrodes (termed colloquially as "torpedodes") suitable for monitoring the tethered bubble within the acoustic cell.

Electrochemical measurements were made using a home-built electrochemical workstation. The electrochemical data, which required only low temporal resolution, were recorded using a Computerboards PCI-DAS1602/16 card. The equipment was interfaced to a PC using HP Vee software. The results of experiments requiring higher temporal resolution were recorded using two different methods. In the first, a Gould 200 MS/s, 100 MHz, 465 digital oscilloscope was employed. The data were transferred to a PC through a RS 232 cable and commercially available software. In the second, data were recorded directly to

(19) Leighton, T. G.; Meers, S. D.; Simpson, M. D.; Clarke, J. W. L.; Yim, G. T.; Birkin, P. R.; Watson, Y. E.; White, P. R.; Heald, G. J.; Dumbrell, H. A.; Culver, R. L.; Richards, S. D. *Acoustical Oceanography*, Proceedings of the Institute of Acoustics; Leighton, T. G., Heald, G. J., Griffiths, H., Griffiths, G., Eds.; Institute of Acoustics: St. Albans, U.K., 2001; Vol. 23, No. 2, p 227.

(20) Birkin, P. R.; Watson, Y. E.; Smith, K. L.; Leighton, T. G.; Simpson, M. D. *Acoustical Oceanography*, Proceedings of the Institute of Acoustics; Leighton, T. G., Heald, G. J., Griffiths, H., Griffiths, G., Eds.; Institute of Acoustics: St. Albans, U.K., 2001; Vol. 23, No. 2, p 242.

(21) Denuault, G. *Chem. Ind.* (*London*) **1996**, *18*, 678.

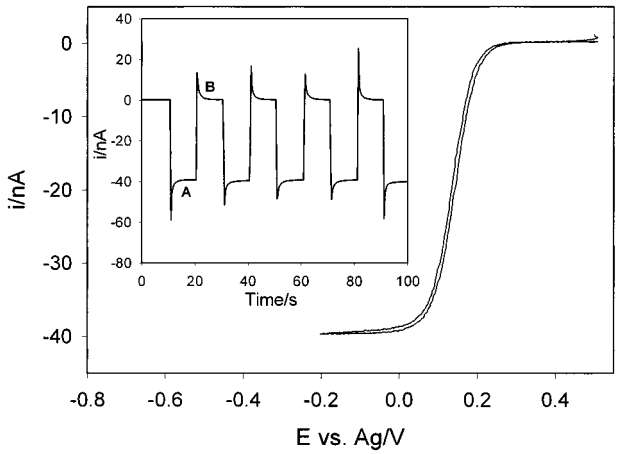

Figure 2. Plot showing the cyclic voltammogram of the microelectrode tip (25 μm diameter Pt) recorded at 10 mV s^{-1}. The anaerobic solution contained 10 mmol dm^{-3} $[Fe(CN)_6]^{3-}$ in 0.2 mol dm^{-3} $Sr(NO_3)_2$. The temperature of the solution was 18−22 °C. The inset in the plot shows a series of potential steps from −200 mV vs Ag (A) to 500 mV vs Ag (B).

a PC over a 2−3 s period at high sample rates using the Computerboards PCI-DAS1602/16 card.

Figure 1 shows a schematic representation of the acousto-electrochemical cell employed to study surface waves on a gas/liquid interface of a bubble. The cell consisted of poly(methyl methacrylate) walls attached to a Mylar loudspeaker. This enabled sufficient room for a glass rod to support a bubble, a hydrophone, electrodes, and visual observation of the phenomena occurring within the cell. In an effort to reduce noise on the electrochemical signal, the electrical connections to the loudspeaker coil were insulated using silicon adhesive and a piece of acetate to act as a "cap" over the connection wires. The bubble was suspended on a glass rod (diameter ca. 6 mm). The rod itself was fabricated with a slight "dimple", which increased the ease of maintaining and isolating a single bubble on the end of the rod. Air bubbles were injected into the solution with a syringe and needle and ranged in radii from ca. 2.5 to 1.5 mm.

A current follower enabling both high gain (up to 1×10^8 V A^{-1}) and low noise acquisition of the experimental data was used. An (*x*, *y*, *z*) Newport micrometer and stage (with 25 mm travel and 10 μm resolution in the *z* direction and 16 mm travel with 10 μm resolution in the *x* and *y* directions) was used to position and move the microelectrode around the cell in order to get an accurate idea of the relative position of the microelectrode. The sound source consisted of a loudspeaker built into the base of the cell. The speaker was driven with the appropriate sound frequency using a TG 101 programmable 10 MHz DDS function generator. A Bruel and Kjear 8103 hydrophone and a Bruel and Kjear 2635 charge amplifier were used to measure and amplify pressure signals, respectively. All electrochemical experiments were performed in a Faraday cage.

All solutions were made using water purified through a USF Elga Elect 5 water purification system. This system produced pure water with a resistivity of typically >15 MΩ cm. Strontium nitrate ($Sr(NO_3)_2$ 99% A.C.S. Reagent, Aldrich) and potassium ferricyanide ($K_3[Fe(CN)_6]$ 99.5% A.C.S. Reagent, Sigma) were used as received.

Results and Discussion

The electrochemistry of the $Fe(CN)_6^{3-/4-}$ redox couple has been studied under a variety of different conditions. Pletcher and Beriet reported that the kinetics of this redox system could be influenced by the ionic strength of the supporting electrolyte.[22] To maintain facile and reproducible electrochemistry, all experiments were carried out employing a solution of $Fe(CN)_6^{3-}$ in 0.2 mol dm^{-3} $Sr(NO_3)_2$. Figure 2 shows the cyclic voltammetry of $Fe(CN)_6^{3-}$ recorded for a 25 μm diameter microelectrode within 0.2 mol dm^{-3} $Sr(NO_3)_2$ aqueous solution. Figure 2 shows that the electrochemistry is well-defined with an extended plateau region below 0 V versus Ag. The inset in Figure 2 shows a series of potential steps from −0.2 to 0.5 V versus Ag. This experiment shows that the steady-state current recorded under mass transfer limited conditions (−0.2 V vs Ag) was reproducible and stable with respect to time.

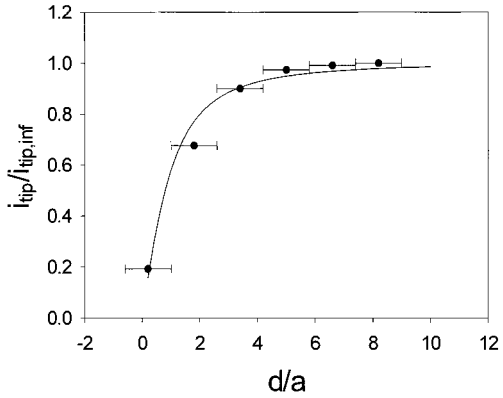

Figure 3. Plot showing how the normalized current varies as a function of distance as the microelectrode (25 μm diameter Pt) was brought up manually to the gas/liquid interface of a tethered bubble. The solution contained 5 mmol dm^{-3} $[Fe(CN)_6]^{3-}$ in 0.2 mol dm^{-3} $Sr(NO_3)_2$. The electrode was held at −0.2 V vs Ag. The aerobic solution was not thermostated. The solid line in the figure represents the curve predicted by simulation. The error bars were calculated assuming an accuracy in the *x* axis of ±10 μm.

To investigate the motion of the bubble wall when irradiated with sound, the tip of the microelectrode was first positioned, using the micrometer and stage, next to the gas/liquid interface of the bubble wall. Figure 3 shows the normalized current ($i_{tip}/i_{tip,inf}$) recorded for a 25 μm diameter microelectrode plotted as a function of distance as the microelectrode approached the bubble wall. The solid line represents the current predicted under these physical conditions (assuming negative feedback) as determined by Denuault and Amphlett.[23] The fit between the experimental data and the prediction is acceptable considering the resolution of the technique employed. In each experiment, where the oscillation of the interface was monitored, the microelectrode was moved toward the interface until the steady-state current was observed to be hindered by ca. 50−75%. This corresponds to a tip to bubble wall distance of ca. 5−10 μm.

Figure 4 shows the response of a microelectrode positioned next to the air/liquid interface of a bubble in the absence and presence of sound irradiation, which was tuned to the bubble resonance using the shimmer technique described above. At $t = 0$, the electrode potential (0.5 V vs Ag) allows no reduction of the $[Fe(CN)_6]^{3-}$ species, but at $t = 20$ s the potential was stepped to −0.2 V versus Ag (corresponding to mass transfer controlled conditions). After the expected current−time transient, the reduction current relaxes to steady state. The distance from the microelectrode to the bubble wall was fixed, except for two step changes (ca. 20 μm), which are marked by A_1 and A_2. At each, the current falls as the bubble wall was approached as a result of hindered diffusion to the microelectrode. For the remainder of the figure, the microelectrode was fixed with respect to the position assumed by the wall when the bubble was not pulsating

(22) Beriet, C.; Pletcher, D. *J. Electroanal. Chem.* **1993**, *361*, 93.

(23) Amphlett, J. L.; Denuault, G. *J. Phys. Chem. B* **1998**, *102* (49), 9946.

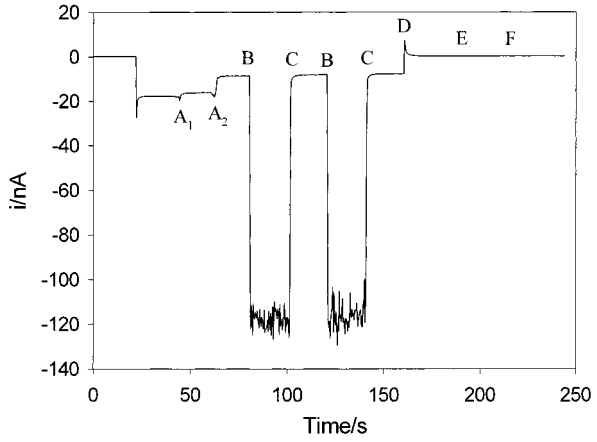

Figure 4. Plot showing the current−time trace recorded for a microelectrode approaching a tethered bubble in the absence and presence of sound irradiation. A_1 and A_2 indicate manual positioning of the microelectrode toward the bubble wall. B and C represent the initiation and termination of sound irradiation of the bubble driven into oscillation (1.2835 kHz), respectively. D represents the point where the potential of the microelectrode was changed from −0.2 V vs Ag (a potential corresponding to mass transfer limiting steady-state conditions) to 0.5 V vs Ag (corresponding to no reduction of the $[Fe(CN)_6]^{3-}$). E and F show the times when sound irradiation was commenced and terminated, respectively. The solution conditions are identical to those reported in Figure 3.

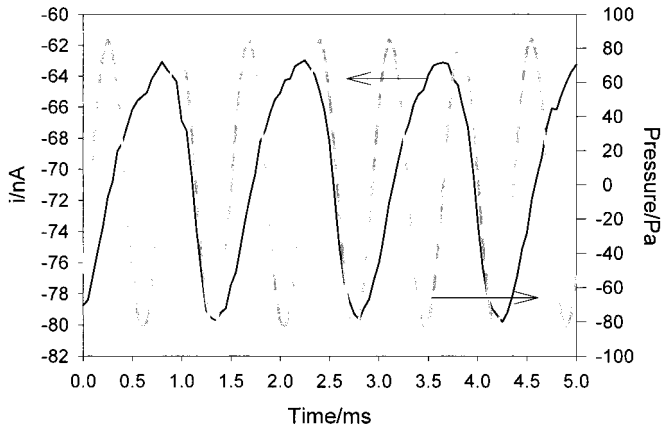

Figure 5. Plot showing the temporally resolved current (black line) and pressure (gray line) traces obtained for a bubble driven to oscillate by a 1.3985 kHz sound field shown as a function of time. The solution conditions are identical to those reported in Figure 3.

(ca. 5−10 μm tip to bubble wall distance). At B, the sound irradiation of the bubble was commenced. An immediate (on this time scale) rise in the current can be seen, indicating that the motion of the bubble wall induces additional mass transfer enhancement to the microelectrode tip through convection of the surrounding liquid. The enhancement in mass transfer is significant with a mass transfer coefficient of 0.025 cm s^{-1}. However, if the sound irradiation of the bubble was terminated (see C), the current immediately fell back to the steady-state value in the absence of forced convection. If the process was repeated, a similar enhancement in mass transfer was observed. To prove that the response of the microelectrode was a direct result of mass transfer enhancements caused by bubble oscillation, the sound irradiation process was repeated when the electrode potential was changed to +0.5 V (D). At this potential, no reduction of the $[Fe(CN)_6]^{3-}$ redox species occurred (see Figure 4, E and F). Under these conditions, no enhancement in mass transfer was observed when the bubble was made to oscillate by exposure to sound. This shows that the signal observed in the presence of sound was a direct result of bubble wall motion and not erroneous electrical noise from the loudspeaker coil.

Figure 5 shows the current−time trace and pressure−time trace recorded simultaneously for a bubble driven to oscillation. In this case, the temporal resolution of the equipment employed was such that the pressure wave and the current−time transient could be resolved. Figure 5 suggests that the current signal is predominantly at half the frequency of the applied sound field (f_p = 1398.5 Hz), which is confirmed by the fast Fourier transforms (FFTs) of both (Figure 6). This is the frequency at which Faraday waves would be set up ($f_p/2$ = 699.25 Hz) and is suggestive that these contribute strongly to the current signal. It is also possible to see a small contribution to the current at the fundamental (f_p = 1398.5 Hz) drive frequency. This implies that as well as the surface wave the microelectrode is able to detect the breathing mode of the bubble wall. The pressure signal recorded from the hydrophone shows no contribution at 699.5 Hz. This suggests that the surface wave motion of the bubble wall does not emit strongly into the solution as expected.

Figure 7 shows two still images of a bubble tethered to a glass rod in the apparatus employed here. The top image (a) shows the bubble in the absence of sound irradiation, while the lower image (b) shows an image of the same bubble excited into oscillation by an acoustic driving signal. Figure 7b shows the presence of surface distortions as the result of Faraday wave motion of the interface.

To verify whether Faraday waves are indeed responsible for the current oscillations observed, an experiment was conducted to determine whether the threshold acoustic pressure required to produce a current component at $f_p/2$ was the same as that required to stimulate Faraday waves. Figure 8 compares the predicted threshold pressure for the two relevant oscillating modes with the measured threshold pressures required to detect $f_p/2$ in the electrochemical signal. The actual pressure threshold for this was measured once the bubble had been knocked off the glass rod. This was necessary as the bubble itself would affect the acoustic pressure measured in the presence of the bubble. Hence, the pressure can only be measured in the absence of the bubble but without altering any other experimental parameters. To determine the pressure threshold for the onset of Faraday wave motion of the bubble wall, the current was monitored as a function of time. The frequency of the sound field was initially set so that no current enhancement or current−time oscillation was observed in the presence of sound. The pressure amplitude was set at a constant value, and the frequency of the sound field was increased until a characteristic component in the current−time data at half the driving signal ($f_p/2$) was noted. The process was then repeated starting from a higher frequency and moving down. The frequency at which current−time oscillation at $f_p/2$ occurred was again noted. This process was repeated at a number of different driving pressures. The pressure threshold exhibits a minimum around the resonant frequency of the bubble (see Figure 8). This is expected if Faraday waves are the source of the $f_p/2$ component in the current. As described in the opening section, as the driving frequency becomes further from resonance, the amplitude of wall pulsation will decrease. If one is already at the threshold for Faraday wave generation,then this frequency shift will require the corrective measure of

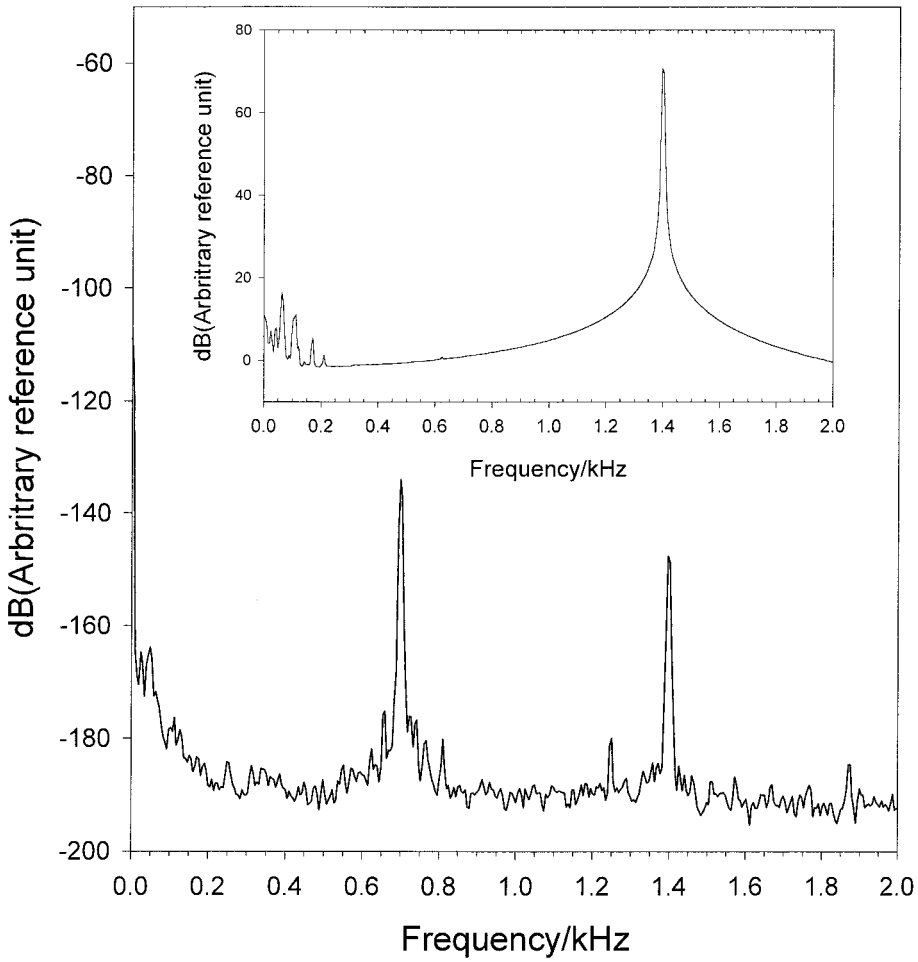

Figure 6. Plot showing the frequency analysis of the current−time data shown in Figure 5. The inset in the figure shows the frequency analysis of the pressure−time data shown in Figure 5. Note that the *y* axis (dB) represents 10 log(*s*/arbitrary unit) where *s* is the power spectral density calculated from FFT analysis of the time series data.

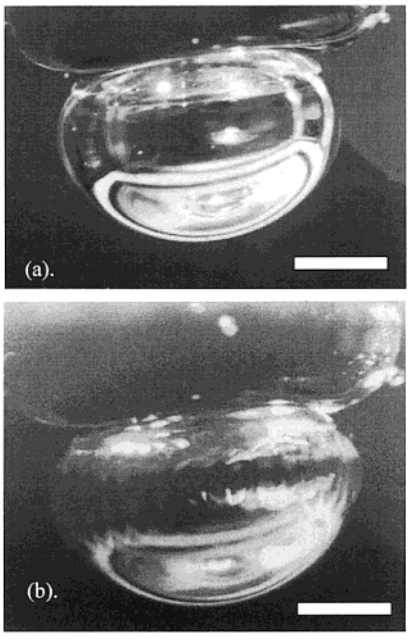

Figure 7. Pictures showing a tethered bubble in the absence of sound irradiation (a) and forced to oscillate by an appropriate sound field (b). The scale bar indicates 1.5 mm.

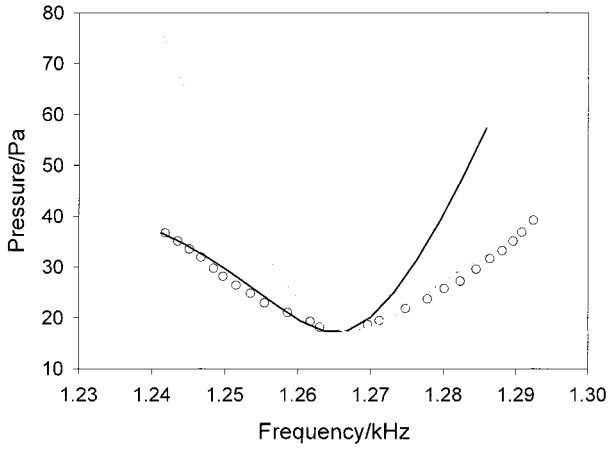

Figure 8. Plot showing the onset of Faraday waves (○) detected using the electrochemical detection method described in the text. The lines represent the pressure threshold for n (the order of the mode) = 15 (black line) and $n = 16$ (gray line) modes of oscillation. The pressure thresholds were calculated using eq 1 and assuming a surface tension of 60 mN m^{-1}, a speed of sound of 1480 m s^{-1}, a viscosity of 8.91×10^{-4} kg m^{-1} s^{-1}, a hydrostatic pressure of 101 kPa, a polytropic index of 1.38, a vapor pressure of 3.54 kPa, and a density of 1000 kg m^{-3}. The solution conditions are identical to those reported in Figure 3.

increasing the amplitude of the driving sound field, to return the bubble to the threshold condition. Final evidence is obtained by plotting in Figure 8 the theoretical prediction for the pressure field amplitude required to generate surface waves in resonant bubbles. The pressure threshold can be calculated by modifying the amplitude threshold derived by Francescutto and Nabergoj to

accommodate the desired pressure threshold prediction (eq 1).[14,16]

$$P_T = R_0^2 \rho C_T[(\omega_0^2 - \omega^2)^2 + (\omega^2 d_{tot})^2]^{0.5} \quad (1)$$

Here, P_T represents the pressure threshold, R_0 is the equilibrium bubble radius, ρ is the density of the medium, C_T is the critical dimensionless amplitude threshold,[16] ω_0 is the resonant angular frequency of the bubble, ω is the driving angular frequency, and d_{tot} is the dimensionless damping coefficient. The two modes ($n = 15$ and 16), which lie around the bubble resonance giving the lowest threshold excitation pressure, are shown. These have frequencies[24] close to $f_p/2$. The agreement between the experimental data and the lowest theoretical threshold for the frequency in question is pleasing. However, the model is extremely sensitive to the physical parameters, particularly the surface tension, entered. In this case, a value of 60 mN m^{-1} was employed. This is close to the measured value for the system of 58 mN m^{-1} and is acceptable considering the assumptions made in the comparison between the theory and the experimental data (e.g., the theory assumes a spherically symmetric bubble while in the experiment the presence of the glass rod will compromise this assumption). The mode corresponding to the lowest threshold energy changes as one moves from above to below the bubble resonance frequency (e.g., $n = 16$ at $\omega > \omega_0$ and $n = 15$ at $\omega < \omega_0$).

(24) Maksimov, A. O.; Leighton, T. G. *Acta Acust.* **2001**, *87* (3), 322.

Conclusions

The results presented here demonstrate that oscillation of the gas/liquid interface of a bubble wall driven to oscillate by an acoustic driving signal can be successfully monitored using a novel electrochemical approach. The low-resolution SECM technique has successfully recorded the oscillation of the interface of a bubble wall. The strongest oscillations reported here are characteristic of Faraday waves on the surface of the bubble. Pressure threshold measurements, frequency analysis of the current−time signals, and photographic data provide evidence for Faraday waves on the gas/liquid interface of a tethered bubble.

LA0111001